JOURNAL OF GEOPHYSICAL RESEARCH, VOL. 103, NO. C11, PAGES 24,881-24,890, OCTOBER 15, 1998

Collision of anticyclonic, lens-like eddies with a meridional western boundary

L. Zavala Sansón,[1] F. Graef, and E. G. Pavía

Centro de Investigación Científica y de Educación Superior de Ensenada
Ensenada, Baja California, México

Abstract. The collision of anticyclonic, lens-like eddies with a meridional western boundary is investigated as a function of two independent, nondimensional numbers: $\beta = \beta_0 R/f_0$ and $\varepsilon = \omega/f_0$, where f_0 and β_0 are the Coriolis parameter and its rate of change with latitude, respectively, both evaluated at the reference latitude, R is the eddy's radius, and ω is its angular frequency. The numerical experiments show that in all cases there is a southward expulsion of mass proportional to both β and ε, which is estimated during the eddy-boundary interaction. The eddies are invariably deformed with the initial collision, but afterward, they reacquire a new circular shape. There is a meridional translation of the eddy along the boundary which depends exclusively on the initial ratio $r = \varepsilon/\beta$. If $r > 1$, the eddy goes southward, but if $r < 1$, the eddy goes northward first and then southward. As the eddy loses mass and reacquires a new circular shape, there is a readjustment of β and ε such that β decreases because its radius becomes smaller and ε increases by energy conservation. This implies that the eddies ultimately migrate southward. A formula derived for the meridional speed of the center of mass of the eddy is consistent with the numerical results. A physical interpretation shows that after collision a zonal force is exerted on the eddy by the wall which is balanced by a meridional migration. Nonlinearities induce a southward motion, while high β values could produce northward motion, depending on the mass distribution along the wall.

1. Introduction

Oceanic eddies continuously migrate westward, in part, owing to β, which means that eventually they would reach a western boundary. Therefore the study of the collision of anticyclonic, lens-like eddies with a meridional western boundary is of scientific interest. Although this paper does not relate to any particular region, our principal motivation is the collision of anticyclonic vortices with the continental shelf of the Tamaulipas coast in the Gulf of México. For example, the Loop Current regularly produces anticyclonic eddies when "the loop" breaks off from the main current [*Ichiye*, 1962; *Elliott*, 1982]. Once the vortices are isolated, with 100 to 200 km radii [*Vukovich et al.*, 1979], they start to migrate westward, approximately 2 to 3 km d^{-1} [*Elliott*, 1982], until they reach the continental shelf at approximately 23°N, 95.5°W [*Kirwan et al.*, 1988].

We use an ocean model consisting of the shallow water reduced-gravity equations for one active layer on the β plane and a numerical method of solution based on a particle-in-cell (PIC) method. This algorithm has been used succesfully in studies of isolated eddies on an f plane [*Pavía and Cushman-Roisin* 1988, 1990; *Pavía and López*, 1994], but here the model is extended to the β plane and includes a solid boundary. We model the western boundary as a meridional vertical wall. The boundary condition at this wall is of no normal flow, and it is modeled as if the numerical particles rebound elastically from it.

All simulations were initialized with a circular rodon [*Cushman-Roisin et al.*, 1985], i.e., an anticyclonic, lens-like eddy rotating as a solid body with parabolic depth profile on an f plane. The eddy's initial position was chosen far enough from the wall to allow for a short adjustment period in which the "discrete rodon" becomes the numerical westward migrating solution on the β plane. The numerical experiments were designed to study the eddy-wall interaction in parameter space, i.e., as a function of the two independent, nondimensional numbers, β and ε, which measure the eddy's size and intensity, respectively.

The experiments show, in all cases, a southward expulsion of mass proportional to β and ε; and, although

[1]Now at Laboratory for Fluid Dynamics and Heat Transfer, Faculty of Physics, Eindhoven University of Technology, Eindhoven, Netherlands.

Paper number 98JC02547.
0148-0227/98/98JC-02547$09.00

the eddies are invariably deformed with the initial collision, they eventually reacquire a circular shape. More important, we found that after the collision there is a meridional translation of the eddy along the wall that depends exclusively on the initial ratio $r = \varepsilon/\beta$; if $r > 1$, the eddy goes southward, but if $r < 1$ the eddy goes northward first and then southward. We derived a simple formula for this meridional translation of the eddy, which is consistent with the numerical results.

There have been several theoretical and observational studies of the collision of eddies against boundaries. *Rossby* [1948] showed that the effect of the latitudinal variation of the Coriolis parameter over the whole eddy exerts a meridional force directed southward for anticyclones in the northern hemisphere. In an open ocean this force is balanced with a westward motion maintaining a coherent structure [*Cushman-Roisin et al.*, 1990]. However, the presence of the wall stops the westward drift, and thus the eddy is accelerated southward. This effect of the wall over the eddy was pointed out by *Nof* [1984]. Here we show analytically that, in fact, the wall exerts a zonal force on the eddy's center of mass, such that if $\beta \ll 1$, the force is eastward and balanced by a southward motion. This translation is accelerated owing to the meridional β force. Therefore our numerical results for $r > 1$ are in agreement with this mechanism. For $r < 1$ the numerical results do not contradict the analytical results, but they are not conclusive.

Other previous studies about the eddy's migration along free-slip walls consider the image effect, i.e., the influence of the eddy's image necessary to satisfy the no-normal flow boundary condition (see, e.g., *Pierrehumbert* [1980] and *Shi and Nof* [1994], for barotropic and baroclinic eddies, respectively). In these cases a northward (southward) drift is predicted for anticyclonic (cyclonic) vortices. However, this result cannot be applied to strong. lens-like eddies. We should recall that as the effect of nonlinearities increases, the motion is no longer quasi-geostrophic, annulling the existence of the stream function; that is, there is no longer a one-to-one relation between the stream function and the velocity field, and the image effect no longer can be established.

An important process during the collision of anticyclones is the presence of a southward mass expulsion. This has been shown by *Nof* [1988a, b] through simple laboratory experiments. Besides confirming Nof's results, we found that this expulsion plays a decisive role in the evolution of the colliding eddy.

Oceanographic observations of eddy-shelf interaction show no definite pattern for the migration of eddies. *Evans et al.* [1985] show southwestward migration along the isobaths for Gulf Stream warm-core ring 82B. *Kirwan et al.* [1988] identify two anticyclonic eddies in the Gulf of Mexico that collide with the Mexican shelf and report that after the collision both of them undergo a brief adjustment and then migrate northward (but, in fact, after one of the eddies turned away a few kilometers from the slope, it changed its migration from northward to southward). *Vukovich and Waddell* [1991] describe the collision of an anticyclonic eddy with the western slope in the Gulf of Mexico in which the vortex adjusts to an elliptical shape with the major semiaxis oriented meridionally, rotating clockwise, and then migrates southward while decreasing in size. These observational studies serve as motivation and offer guidance to our work; but, obviously, neither this study nor the previous model studies pretend to fully explain these observations. Recall that all model studies rely on drastic simplifications. Perhaps realistic simulations should include advection by coastal currents, topographic effects, interaction with other eddies, and/or other phenomena.

The rest of this paper is organized as follows: In the next section we begin by presenting the model equations, then we describe the particle method and the initialization of the experiments. The main results of this work are presented in section 3, and their discussion constitutes section 4. In section 5 we enumerate the conclusions and recapitulate our findings. Finally, in the appendices we explain the implementation of the boundary condition and a quantitative measure of the expelled mass.

2. Ocean Model

The shallow water equations for a $1\frac{1}{2}$ layer model on a β plane are:

$$\frac{\partial u}{\partial t} + u\frac{\partial u}{\partial x} + v\frac{\partial u}{\partial y} - (f_0 + \beta_0 y)\, v = -g'\frac{\partial h}{\partial x}, \quad (1)$$

$$\frac{\partial v}{\partial t} + u\frac{\partial v}{\partial x} + v\frac{\partial v}{\partial y} + (f_0 + \beta_0 y)\, u = -g'\frac{\partial h}{\partial y}, \quad (2)$$

$$\frac{\partial h}{\partial t} + \frac{\partial (hu)}{\partial x} + \frac{\partial (hv)}{\partial y} = 0, \quad (3)$$

where x and y are eastward and northward coordinates, respectively; u and v are the corresponding velocity components; h is the active layer depth; f_0 and β_0 are the Coriolis parameter and its rate of change, respectively, and $g' = g(1 - \rho_1/\rho_2)$ is the reduced gravity, in which ρ_1 and ρ_2 are the densities of the active and inactive layers, respectively, and $\rho_1 < \rho_2$ (see Figure 1).

Equations (1)–(3) are nondimensionalized with the tangential speed ωR for the velocities, R for the horizontal length scale, $H_m \sim R^2\omega f_0/g'$ for the depth scale, and f_0^{-1} for the timescale. We then obtain the following nondimensional system:

$$\frac{\partial u}{\partial t} + \varepsilon\left(u\frac{\partial u}{\partial x} + v\frac{\partial u}{\partial y}\right) - v - \beta y v = -\frac{\partial h}{\partial x}, \quad (4)$$

$$\frac{\partial v}{\partial t} + \varepsilon\left(u\frac{\partial v}{\partial x} + v\frac{\partial v}{\partial y}\right) + u + \beta y u = -\frac{\partial h}{\partial y}, \quad (5)$$

$$\frac{\partial h}{\partial t} + \varepsilon\left(\frac{\partial (hu)}{\partial x} + \frac{\partial (hv)}{\partial y}\right) = 0, \quad (6)$$

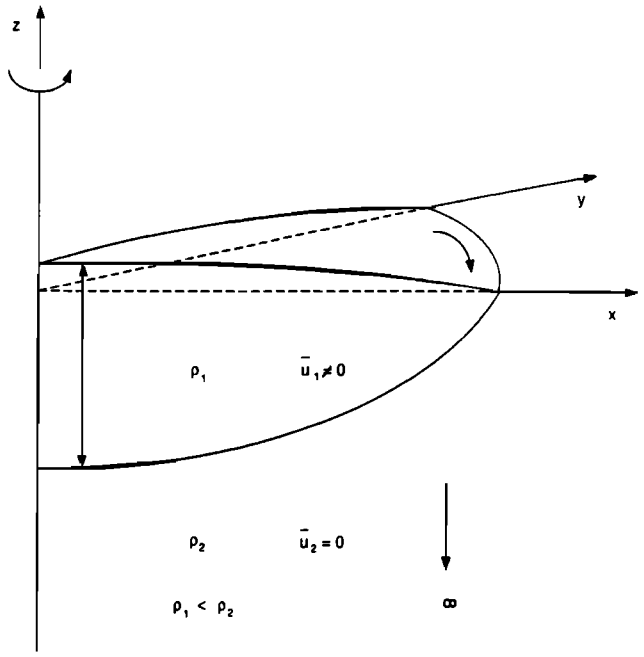

Figure 1. Schematic view of the frontal eddy model.

where the nondimensional parameters are

$$\varepsilon = \frac{\omega}{f_0}, \quad \beta = \frac{\beta_0 R}{f_0}, \tag{7}$$

where ω is the eddy angular frequency and R is the eddy radius.

2.1. Numerical Implementation

In the PIC method used to solve (1)–(3) the active layer is approximated by a large number N of particles, whereas the passive layer is represented by regions with no particles. Essentially, this method solves at every time step the following system for each particle:

$$\frac{Dx_i}{Dt} = u_i, \tag{8}$$

$$\frac{Dy_i}{Dt} = v_i, \tag{9}$$

$$\frac{Du_i}{Dt} = (f_0 + \beta_0 y_i)v_i - g'\left(\frac{\partial h}{\partial x}\right)_i, \tag{10}$$

$$\frac{Dv_i}{Dt} = -(f_0 + \beta_0 y_i)u_i - g'\left(\frac{\partial h}{\partial y}\right)_i, \tag{11}$$

$i = 1, 2, \ldots, N$; here (x_i, y_i) and (u_i, v_i) are the position and velocity of the ith particle, respectively. Since each particle keeps its volume constant, the continuity equation (3) is implicitly satisfied. Then, we have control over the particle's positions and velocities at all times. From them we obtain the Coriolis force, but the pressure gradient force is evaluated by first extrapolating the particles's contribution to the h field over an Eulerian grid, therein obtaining the spatial derivatives by finite differences, and then interpolating back the pressure gradients to the particles positions. We use a Hanning filter for the h field (see *Pavía and Cushman-Roisin* [1988] for details).

The kinematic boundary condition at rigid walls is that there be no flow normal to the boundary. In our Eulerian-Lagrangian method we implement this condition assuming that the particles rebound ellastically from the wall, as explained in Appendix A.

2.2. Model Initialization

All simulations were initialized with a circular rodon [*Cushman-Roisin et al.*, 1985], which is an anticyclonic, lens-like eddy rotating as a solid body with parabolic depth profile. Using a frame of coordinates with the origin at the eddy's center, the depth and velocity fields are

$$h = H\left(1 - \frac{x^2 + y^2}{R^2}\right), \tag{12}$$

$$u = \omega y, \tag{13}$$

$$v = -\omega x, \tag{14}$$

for $0 \leq x^2 + y^2 \leq R^2$, and $h = u = v = 0$ for $x^2 + y^2 > R^2$, where H is the maximum depth given by

$$H = \frac{R^2}{2g'}\omega(f_0 - \omega), \tag{15}$$

with $\omega < f_0$ [*Cushman-Roisin et al.*, 1985]. In the numerical code we prescribe ω and R, whereas H is obtained from (15). In all experiments the reduced gravity was kept constant with a value of 10^{-2} m s^{-2}.

The numerical experiments start with a short adjustment period (5 to 20 days) in which the exact solution on the f plane becomes the numerical westward migrating solution on the β plane, so the eddy's initial position was chosen far enough from the wall.

The physical domain of the experiments was a 990 $\times$ 990 km^2 ocean with a resolution of $\Delta x = 10$ km and a radius of deformation of about 30 km. When we increased the resolution to $\Delta x = 5$ km and thus the number of particles increased fourfold, only a small difference in the results was found. However, since this is at a much higher computational cost, we chose the original grid and number of particles, $N = 10,981$. An empirical rule is that in order to have a robust algorithm, we must have 10 to 15 particles per cell in the active region [*Pavía and Cushman-Roisin*, 1988]. In contrast to these authors, we use particles of different volume; at $t = 0$ they decrease in size from the center to the edge of the eddy to try to ensure that even the shallowest regions are well resolved. This is preferable than an explicit check on the number of particles per cell, which would be computationally very expensive.

3. Numerical Results

We performed two different experiments. In the first experiment we try to find the influence of the four parameters, f_0, β_0, ω, and R, on the eddy's behavior when it senses the wall. This means that we chose arbitrary values for these parameters, even if they do not correspond to very realistic cases. In the second experiment we use typical values of f_0 and β_0 from a fixed latitude and ω and R for oceanic eddies.

The position in the ε versus β space of each of the 18 runs of the first experiment is shown in Figure 2a. In general, we observed the following behavior: (1) When the eddies touch the wall, invariably a southward loss of mass is produced. (2) Just after the collision, the eddies are deformed at the west side owing to the presence of the wall. This deformation is proportional to their zonal velocity. After the initial impact the remanent eddy shows a clear core which adjusts to an approximately circular shape with new ε and β. The west side deformation is more evident when β is large; when this is the case, the eddy seems to take an elongated shape. (3) The eddies' core translates meridionally southward when initially, $r > 1$ ($\varepsilon > \beta$), and northward in the beginning and then southward when initially, $r < 1$ ($\varepsilon < \beta$).

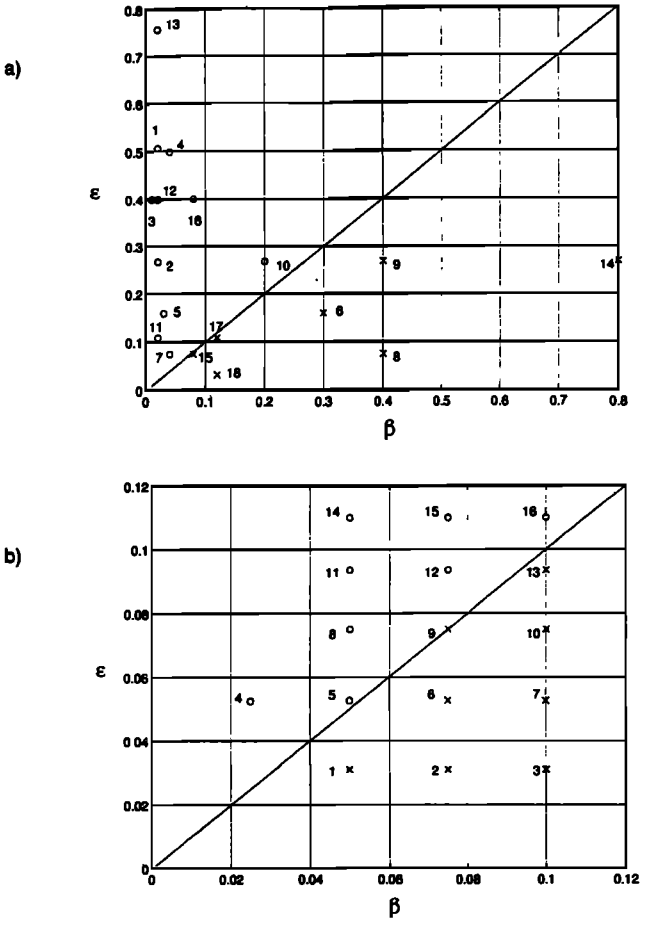

Figure 2. Parameter space showing the runs of (a) experiment 1 and (b) experiment 2. The runs marked with circles (crosses) are those when the eddy migrates to the south (north).

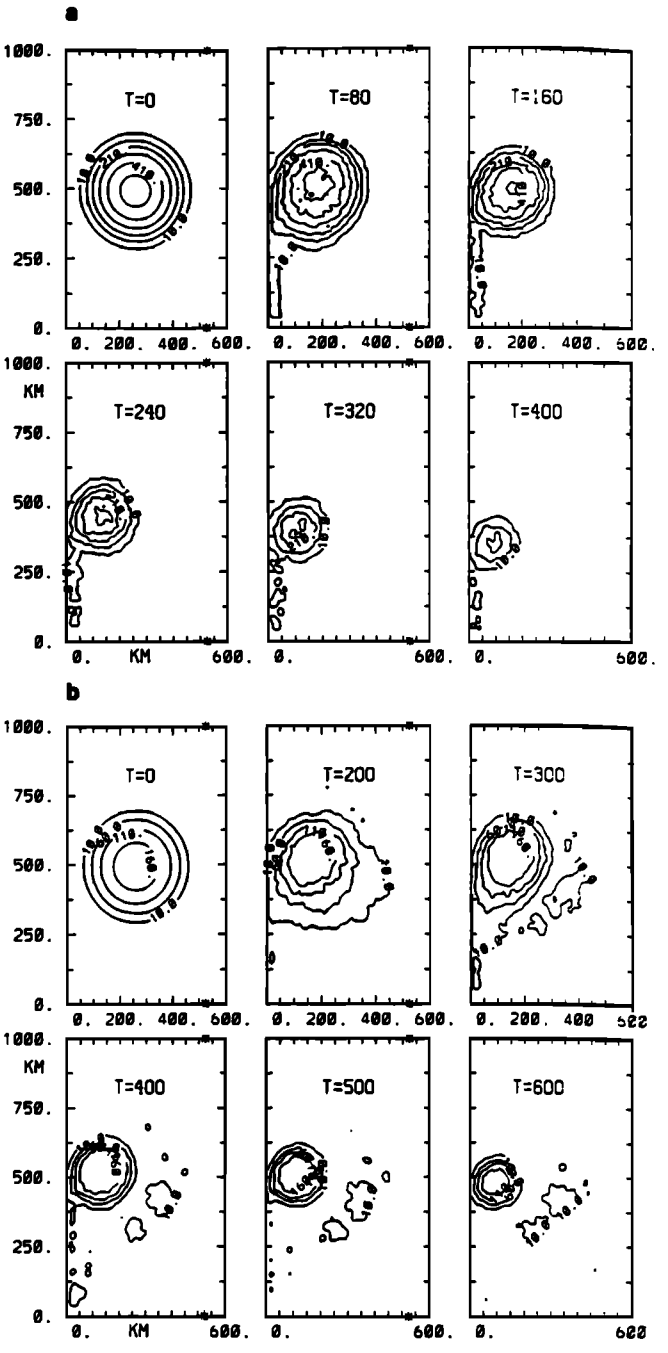

Figure 3. (a) Depth contours of case 12 from experiment 2 (with two independent nondimensional numbers $\beta = 0.075$, $\varepsilon = 0.095$) shown at different times (days). (b) Depth contours of case 2 from experiment 2 ($\beta = 0.075$, $\varepsilon = 0.03$) shown at different times (days).

In the second experiment we fixed the planetary vorticity f_0 and its gradient β_0 at a latitude of 23°N [$f_0 = 5.66 \times 10^{-5}$ s^{-1}, $\beta_0 = 2.09 \times 10^{-11}$ (m s)$^{-1}$], where the Loop Current eddies are likely to interact with the continental shelf [*Kirwan et al.*, 1988; *Vukovich and Waddell*, 1991]. In this experiment we only change the radius and the angular speed with realistic values

for oceanic eddies. The position of the runs of this experiment in the ε versus β space is shown in Figure 2b.

A couple of examples of the evolution of the eddy-wall interaction from the second experiment are presented in Figure 3, where we show the depth contours of the numerical solution at selected times. Run 12 ($\varepsilon = 0.095$, $\beta = 0.075$) has $\varepsilon > \beta$, and we can observe clearly the southward mass expulsion, the eddy's circular shape after collision, and its southward migration (Figure 3a). Run 2, with $\varepsilon = 0.03$ and $\beta = 0.075$, i.e., $\beta > \varepsilon$, shows a greater loss of mass (however, the process is more complicated) and a more evident west side deformation, but now the initial movement is northward and afterward, southward (Figure 3b). In both cases the southern, northern, and eastern boundaries are open. In run 2 the time intervals are larger than in run 12 because the eddy is weaker. Although we consider the entire mass expulsion process to be important, some of the smallest blobs might not be well resolved numerically.

We should mention that in this experiment we can make better quantitative measurements than in the first one. In particular, we can measure more easily the southward loss of mass.

3.1. Meridional Migration: Initial ε and β

We have found that eddies with $\varepsilon > \beta$ move southward and those with $\beta > \varepsilon$ move initially northward and, afterward, southward. This behavior is confirmed in Figure 4, where we plot the position of the eddy's core at different times for runs 2 ($\beta > \varepsilon$) and 12 ($\beta < \varepsilon$) of the second experiment; the northward displacement of run 2 is small, with respect to the initial eddy's radius, but is evident. We define the eddy's core as the fluid whose depth is such that $h > 0.1H$; that is, we exclude the expelled fluid of small depth.

The northward movement decreases when the eddy loses mass, and the eddy is forced to adjust to a new shape with different ε and β, as discussed in section 3.2.

3.2. Evolution of the Collision: Changes in ε and β

The southward mass expulsion is directly related to the nondimensional numbers ε and β; that is, the larger they are, the greater is the mass expulsion. Figure 5 shows the ε versus β space of the second experiment with the percentage of mass expelled 150 days after the eddy collided with the wall. We found that the expelled mass is approximately proportional to ε and β. The method used to measure the expelled mass is explained in appendix B.

Furthermore, after the collision and deformation the remanent eddy reacquires a circular shape, so we assume that we can identify it with new values of β and ε. The loss of mass implies that β decreases because the radius decreases and that ε increases owing to energy conservation, as discussed in section 4.3. We can obtain the new β once we approximate the new radius because $\beta = \beta_0 R/f_0$. To get the new ε, we look for the new characteristic angular speed. If we start from the maximum depth of a circular rodon [see (15)], with H and R known, we can solve for ω and then compute $\varepsilon = \omega/f_0$. Thus we measure the maximum depth and the approximated radius for each case of the second experiment in order to get the new β and ε.

One of the main results of this work is summarized in Figure 6. It shows the initial and final position of

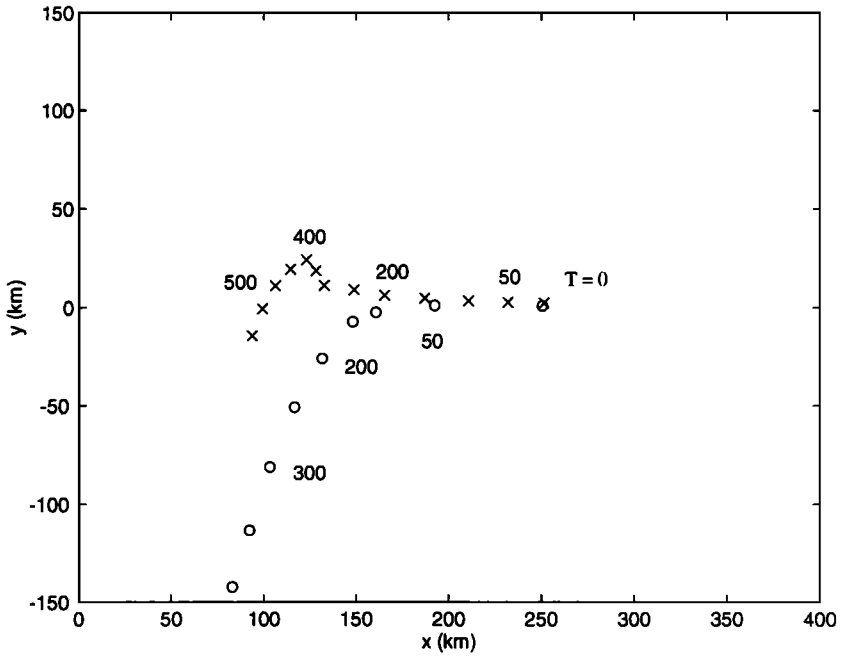

Figure 4. Positions at different times (days) showing the meridional migration of the main eddy of runs 2 (crosses) and 12 (circles) from experiment 2.

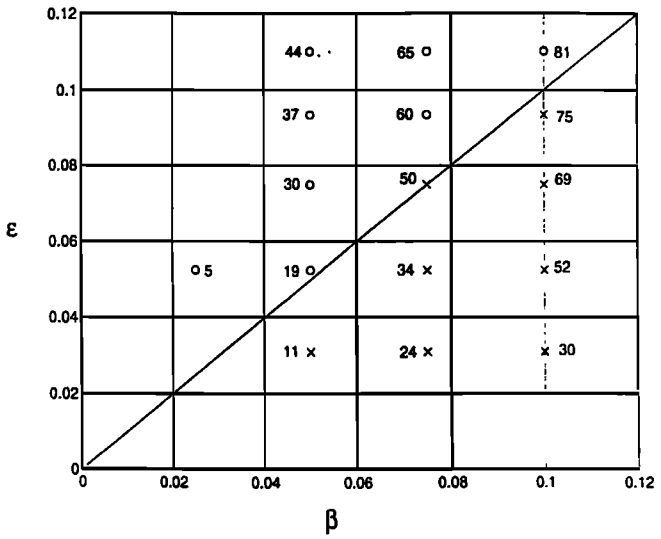

Figure 5. Percentage of mass expelled from the runs of experiment 2, 150 days after the collision.

the eddy (150 days after collision), in parameter space, joined with a straight line. Figure 6 clearly shows that ε increases and β decreases such that the final position of the eddy in parameter space is always in the region where the eddies move southward ($\varepsilon > \beta$).

4. Discussion

4.1. Southward Mass Expulsion

The presence of the wall stops part of the eddy's flow at the southwest side because of its anticyclonic rotation. Thus the fluid near the wall tends to be expelled southward.

This process has been studied analytically by *Nof* [1988a, b] for barotropic and baroclinic eddies barely touching a wall on an f plane. Anticyclonic eddies tend to leak fluid on their right-hand side (looking offshore), whereas cyclonic eddies leak on their left-hand side. In addition, *Nof* [1988b] presents physical evidence of this phenomenon by means of simple laboratory experiments.

In this study we found numerically that the southward mass expulsion persists on the β plane and, more important, increases as β and ε do because the vortex is continuosly pushed toward the wall. This pressing is due to the eddy's westward speed before the collision, which is $O(\beta f_0 R_d^2/R)$, where R_d is the deformation radius [*Cushman-Roisin et al.*, 1990]. Let us assume that the mass expelled after a period $\omega^{-1} = (\varepsilon f_0)^{-1}$ has a width $O(\beta R_d^2/\varepsilon R)$, a length $O(R)$, and a depth $O(\varepsilon H)$ (see also *Shi and Nof* [1994] for a similar analysis). Then, the rate of expelled volume (cubic meters per second) is $O(\beta\varepsilon f_0 H R_d^2)$. Considering the initial volume of the eddy as $O(HR^2)$, the percentage of expelled mass per second is $P = 100 \times O[\beta\varepsilon f_0 (R_d/R)^2]$. Using the deformation radius $R_d = (g' H_m)^{1/2}/f_0$, where H_m is the mean depth of a rodon (see section 2), the percentage becomes $P = 100 \times O(\beta\varepsilon^2 f_0)$. Recall that this approximation gives only orders of magnitude that are roughly in agreement with the runs of experiment 2. For instance, the predicted percentages of expelled mass in runs 2 and 12 after 150 days are 5% and 50%, respectively, while values of 24% and 60% were measured (see Figure 5). The differences may be due to changes in β and ε as the eddies lose mass, but orders of magnitude are correct.

4.2. Meridional Migration

In order to understand the eddy's behavior interacting with the wall, we now obtain an analytical expression for the meridional migration. Owing to the problem's complexity, some assumptions are necessary, but the main physical mechanisms are considered. We follow the formalism used by *Ball* [1963] for a rotating fluid lying on a paraboloid. Ball defined the coordinates of the eddy's center of mass and derived the equations for its time evolution. *Killworth* [1983] applied this method to describe the zonal motion of mesoscale eddies in an open ocean, and *Cushman-Roisin et al.* [1990] extended Killworth's results. In this study we consider a semi-infinite plane bounded by a wall and derive the equations of motion for the center of mass of an eddy colliding with it. We then obtain an expression for the meridional migration. Recall that our purpose is not to derive a general formula for the meridional drift but, rather, to understand the physical mechanisms observed in the numerical results.

4.2.1. Formula. In nondimensional form the problem is defined by the momentum equations (4) and (5) and the mass equation (6), together with the boundary

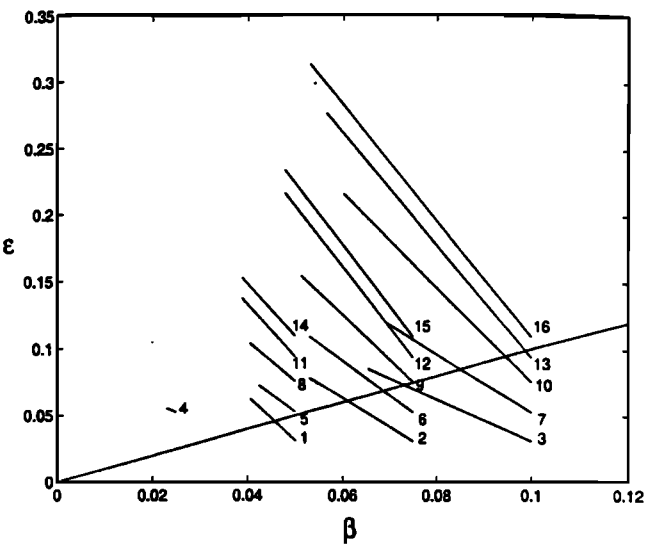

Figure 6. Stick diagram showing initial and final states in the parameter space from experiment 2, 150 days after the collision. Number indicate the run and the initial state.

conditions $u = 0$ at $x = 0$ and $u = v = h = 0$ outside the vortex.

Consider the semi-infinite plane $0 < x < \infty$, $-\infty < y < \infty$ bounded by a meridional vertical wall at $x = 0$. The vortex-wall collision is idealized in Figure 7, where S is the horizontal area where fluid is in motion and ϕ is its material boundary. Note that h is zero along ϕ, except at the wall. Let the eddy's volume

$$V = \int h dS$$

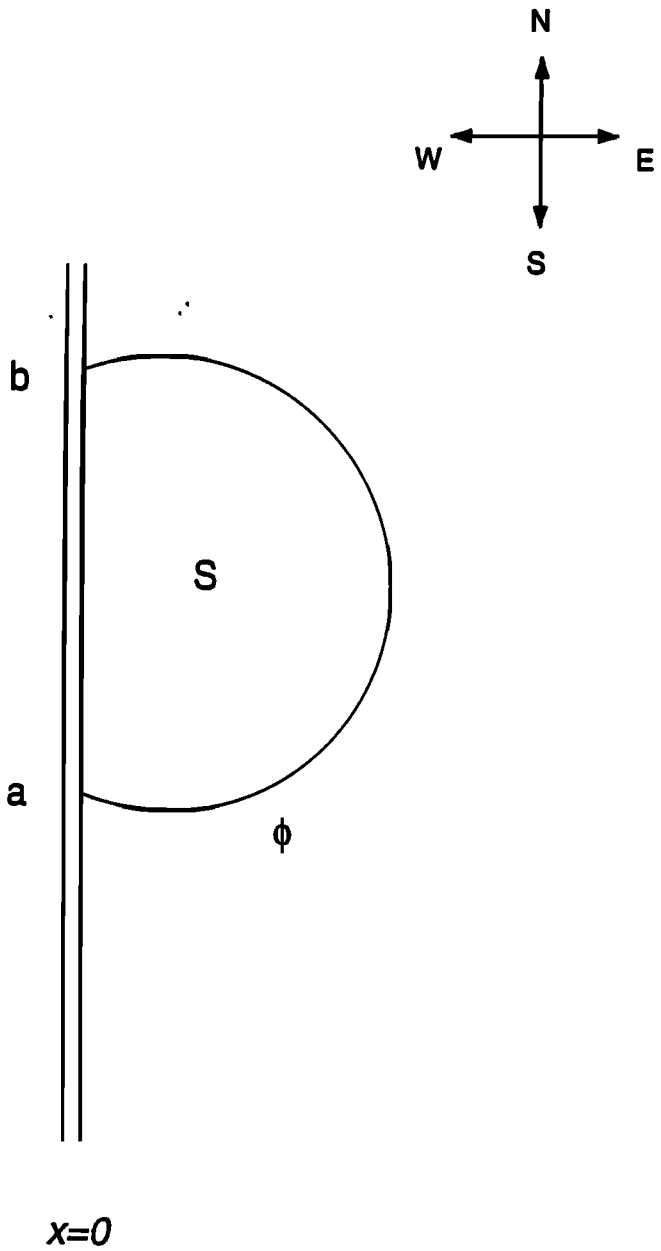

Figure 7. The idealized vortex-wall collision. S is the area where the fluid is in motion, and ϕ is its material boundary; active layer depth h is zero along ϕ, except at the wall (between a and b). Note that the mass expulsion has been neglected.

be a constant ($dV/dt = 0$); that is, the southward mass expulsion is ignored. Note that (6) implies that the whole volume of the fluid in motion is a constant.

The coordinates of the eddy's center of mass are defined as

$$VX = \int xh dS$$

$$VY = \int yh dS.$$

Using the Reynold's transport theorem and (6), we obtain

$$V\frac{dX}{dt} = \varepsilon \int hu dS$$

$$V\frac{dY}{dt} = \varepsilon \int hv dS.$$

Differentiating again and using (4) and (5), we get

$$V\frac{d^2X}{dt^2} - V\frac{dY}{dt} = \frac{\varepsilon}{2}\int_a^b h^2(0,y,t)dy + \varepsilon\beta \int hyv dS \quad (16)$$

$$V\frac{d^2Y}{dt^2} + V\frac{dX}{dt} = -\varepsilon\beta \int hyu dS. \quad (17)$$

The first term on the right-hand-side of (16) appears because of the wall since $h|_{x=0} \not\equiv 0$. This term represents the force exerted by the wall over the vortex during the collision as previously discussed by *Nof* [1984] (see below). The integral of hh_y vanishes since h vanishes at the northern, southern, and eastern boundaries of S.

Because of the wall's presence, the vortex cannot penetrate and $dX/dt \sim 0$. This restriction is the "boundary condition" for the eddy's center of mass imposed by the wall. We examine the validity of this assumption at the end of this subsection. In addition, the geostrophic approximation is used to eliminate u and v from (16) and (17). After some manipulations,

$$-\frac{dY}{dt} = \frac{\varepsilon}{2V}\int_a^b h^2(0,y,t)dy - \frac{\varepsilon\beta}{2V}\int_a^b yh^2(0,y,t)dy + O(\varepsilon^2\beta, \varepsilon\beta^2) \quad (18)$$

$$\frac{d^2Y}{dt^2} = -\frac{\varepsilon\beta}{2V}\int h^2 dS + O(\varepsilon^2\beta, \varepsilon\beta^2). \quad (19)$$

Equation (18) shows the balance of forces on the center of mass in the zonal direction; the force exerted by the wall during the collision is balanced by a meridional translation dY/dt. This effect is similar to the migration of eddies in an open ocean where the southward β force (produced by the imbalance of the Coriolis force within an anticyclonic eddy) is balanced by a westward motion [*Cushman-Roisin et al.*, 1990]. However, there are important differences; the meridional migration can be northward or southward, depending on the sign of the integrals along the boundary on the right-hand side of (18), whereas for open ocean eddies only westward motion is possible.

To illustrate this, consider that for most oceanic

cases, $\beta \ll 1$ and thus the first integral of $O(\varepsilon)$ dominates the second one of $O(\varepsilon\beta)$. The $O(\varepsilon)$ integral is positive, and thus the force exerted by the wall is directed eastward. Then, this force is balanced by a southward meridional migration proportional to ε. This is consistent with our numerical results, where ε shows an influence on the southward motion. With dimensions, the meridional speed is

$$c_m = -\frac{g'}{2f_0}\frac{\int_a^b h^2(0,y,t)dy}{\int hdS} \tag{20}$$

Recall that we neglected the mass expulsion. However, as long as the eddy keeps an approximately circular shape, it can be identified with new β and ε values and the same procedure is applied for each "new" vortex. [Then, as β decreases and ε increases, it reinforces the southward migration given by (20)].

The migration could be northward if β is $O(1)$ and if there is a northern distribution of $h^2(0,y,t)$ along the wall such that the second term on the right-hand side of (18) becomes negative and larger than the first one. This unlikely situation would induce a northward motion of the eddy.

On the other hand, there is no balance of forces in the meridional direction, where only the β force is present accelerating the vortex southward (see (19)). This is also consistent with our numerical results in the case of $\varepsilon < \beta$, where the eddy goes northward first, stops, and then moves southward.

Although (20) gives a physical interpretation of the meridional migration of lens-like eddies, some aspects should be noted. First, the meridional migration depends on the depth field at the wall, $h(0,y,t)$, which is unknown. We are, however, more interested in the sign of c_m than in its numerical value. Second, in order to have a meridional migration, we assumed, based on the numerical results, that the eddy's center of mass does not move in the zonal direction ($dX/dt \sim 0$ and $d^2X/dt^2 \sim 0$). The present analysis therefore cannot be extended to more general situations.

4.2.2. Related studies. As mentioned in section 4.2.1, anticyclonic eddies in an open ocean do not move southward, even though the β force is present, because it is balanced by the eddy's westward translation [*Cushman-Roisin et al.*, 1990]. However, if there is a meridional western wall, the wall stops the eddy's westward translation and thus the β force accelerates it southward. *Nof* [1984] proposed this mechanism in an analytical work of the eddy-wall interaction in a two-layer model, stating that the β force must push the eddy southward. In Nof's analysis a steady state is reached when a northward boundary current at the lower layer balances the β force effect. When the lower layer is at rest (present study), this balance is not possible and the vortex can be accelerated southward (see (19)). In the zonal direction, Nof found that the force exerted by the wall is

$$\frac{g'}{2}\int_a^b h^2(0,y,t)dy$$

but is balanced by the corresponding zonal component of the lower layer. As shown in section 4.2.1, with a motionless lower layer, this force is balanced by a meridional migration (see (18)).

We speculate that the weak northward migration could also be related to the southward mass expulsion, i.e., with the rocket effect mentioned by *Shi and Nof* [1994], where the expelled mass pushes the eddy northward. To explore this possibility, we ran several numerical experiments in which the eddy was placed in contact with the wall from the beginning, as in the work by *Shi and Nof* [1994]. However, in contrast to these authors, our initial fields are frontal while theirs are Gaussian. The results showed a large southward mass expulsion and a weak northward migration. Afterward, the eddies recovered their circular shape and moved southward as before.

On the other hand, barotropic and quasi-geostrophic eddies are dominated by the image effect [*Pierrehumbert*, 1980; *Shi and Nof*, 1994]; that is, along a western wall, anticyclones move northward. *Shi and Nof* [1994] concluded that the same rule could be applied for lens-like eddies. We agree with the former result, where the influence of the undisturbed surrounding fluid might be decisive on the eddy's motion. However, we believe the image effect could not be established for lens-like eddies. In fact, we should recall that as $\varepsilon \to 1$, i.e., as the effect of nonlinearities increases, the motion is no longer quasi-geostrophic and voids the existence of the stream function. The analogy between vortices and electric charges in electrostatics, namely, $\nabla^2\Phi = q$, where Φ is the electric potential (stream function) and q is the electric charge (relative vorticity), which is implied when invoking the image effect, can no longer be established.

4.3. Eddy Readjustment

The meridional movement along the wall is associated to the changes in ε and β due to the mass expulsion. That is, ε increases by energy conservation because as the eddy loses mass, the depth and the potential energy decrease, while the kinetic energy increases. On the other hand, β decreases simply because the radius is decreasing.

After the collision the remanent eddy tends to reacquire a circular shape, and we can expect the northward impulse to diminish. Also, the increasing of nonlinearities induces the final effect to be the southward migration. Note that the β force also decreases, but this does not hinder the southward movement.

5. Conclusions

We have studied the collision of anticyclonic, lens-like eddies with a meridional western boundary by means of a numerical model. A particle-in-cell method is used to solve the reduced-gravity shallow water equations on a β plane. The collision has been explored for the first time in full parameter space, namely, as a function of two independent, nondimensional numbers: $\beta = \beta_0 R/f_0$ and $\varepsilon = \omega/f_0$, which measure the eddy's size and intensity, respectively.

When the eddy collides with the wall, it expels mass to the south. The amount of expelled mass has been estimated, and it is proportional to ε and β (Figure 5). The eddies are invariably deformed with the initial collision, but afterward, they reacquire a new circular shape. There is a meridional translation of the eddy along the boundary that depends only on the initial ratio $r = \varepsilon/\beta$; if $r > 1$, i.e., if initially, nonlinearities dominate over the β effect, the eddy goes southward, and if initially, $r < 1$, the eddy goes northward first and then southward.

To investigate the physical mechanisms of the eddy's behavior, we derived the equations of motion of the eddy's center of mass, which show that the meridional drift is necessary to balance the zonal force exerted by the wall on the eddy (equation (18)). This meridional motion is always accelerated southward by the β force (equation (19)). For $\beta \ll 1$ the force exerted by the wall is directed eastward and the meridional migration is toward the south, given by (20), and proportional to ε, which is consistent with the numerical results. (This is similar to the westward drift of the eddy in an open ocean which balances the southward β force.) The analysis is not conclusive for $r < 1$ because it is not possible to determine the sign of the meridional speed in (18), which depends on the distribution of mass along the wall. However, the numerical results suggest that β is directly responsible for the eddy's deformation because its westward speed is proportional to β. We speculate that this deformation may cause a mass distribution such that the meridional migration becomes northward. Such behavior is observed only when $r < 1$, i.e., $\varepsilon < \beta$.

Therefore the β force and the nonlinearities induce the eddy to move southward, whereas the deformation of the eddy, caused by the collision, might be responsible for its northward motion. Other possible mechanisms for the northward translation, cited by previous authors [e.g., *Shi and Nof*, 1994], are the rocket and image effects. However, for strongly nonlinear eddies, we argue against the latter.

The mass expulsion allows the remanent eddy to reacquire a new circular shape, diminishing the northward impulse. As the eddy loses mass, there is a readjustment of β and ε such that β decreases because its radius becomes smaller and ε increases by energy conservation. This means that the eddy parameters tend to become $r > 1$, and therefore the eddy ultimately migrates southward.

Appendix A: The Boundary Condition

A1. Implementation

The boundary condition of no flow normal to the boundary was implemented in the following way: In a right hand side coordinate system, let us call B the abscisa value of the wall's zonal position, chosen arbitrarily as a meridional line on the grid. Suppose that at time t there is a particle with zonal position x_i such that $x_i(t) > B$, and at the next time step, $x_i(t + \Delta t) < B$; that is, it would cross the boundary. If the particle rebounds ellastically, its zonal position is $x_i^{\text{reb}}(t + \Delta t) = 2B - x_i(t + \Delta t)$, and the velocity component normal to the wall changes sign, $u_i^{\text{reb}}(t + \Delta t) = -u_i(t)$. In other words, the boundary condition is such that the normal velocity of the particle, averaged before and after it hits the wall, is zero. The meridional position and velocity component remain unchanged. This is done very easily within the numerical code with an "if" statement as follows:

```
if x_i(t + Δt) < B then
  x_i(t + Δt) = 2B − x_i(t + Δt)
  u_i(t + Δt) = −u_i(t)
  y_i(t + Δt) = y_i(t + Δt)
  v_i(t + Δt) = v_i(t + Δt)
end if
```

A2. Variations to the Elastic Rebound

One way to test the validity of the boundary condition is to repeat some runs, making the particles rebound in a random direction but preserving the speed magnitude to avoid loss of energy. The results we found with both types of rebound were qualitatively very similar. We also tested some other variations to the boundary condition, for example, replacing the particle to its original position and changing only the sign of the normal velocity component u, repositioning the particle on the boundary and setting u to zero, and changing only the sign of u without any reposition of the particle. In all these variations we found only small changes in the results, but, in general the behavior of the eddy was the same. The reason for this apparent insensitivity to variations of the boundary condition is related to the small changes in the position of the particles when they arrive at the wall. This means that when they rebound, they are repositioned, at most, 0.5 km, while the grid size is 10 km. Thus it is of little importance how we make this repositioning because the overall influence over the grid (and the pressure gradients) is very small. In the cases where we set $u = 0$, the energy is not conserved as in the elastic rebound because we are eliminating one component of the velocity.

Appendix B: Quantitative Measurement of the Expelled Mass

Here we describe how we measured the eddy's mass expulsion in the second experiment. These measure-

ments are approximated because we use a subjective criterion to determine which particles belong to the eddy and which particles have been expelled from it.

The following method was used: We left open the southern boundary, resulting in a loss of particles. If this boundary were closed, the particles would go around in the square ocean and rejoin the eddy with the possibility of affecting its evolution. From a numerical point of view we set to zero the volume of each particle that leaves the southern boundary. Then, 150 days after the collision, we estimated the eddy's radius R_{150} and the position of the maximum depth (x_H, y_H). Finally, we measured the mass contained in the square whose side has a length of $2R_{150}$ and its center is at (x_H, y_H). We could use the circle of radius R_{150}, but it is easier to use the square. The error is negligible because the mass at the perimeter is small compared with the total. A more precise way to make this measurement would be to fit a rodon by least squares [*Pavía and López*, 1994]; however, for the purposes of this investigation the procedure just described yields acceptable results.

Acknowledgments. This research was supported by CICESE and CONACYT under grants 1002-T9111, 4919-E, and 5083-T. The authors want to thank C. Lozano, J. L. Ochoa, M. Stern, and O. Velasco-Fuentes for helpful and stimulating discussions.

References

Ball, F. K., Some general theorems concerning the finite motion of a shallow rotating liquid lying on a paraboloid, *J. Fluid Mech., 17*, 240-256, 1963.

Cushman-Roisin, B., W. H. Heil, and D. Nof, Oscillations and Rotations of elliptical warm-core rings, *J. Geophys. Res., 90*, 11,756-11,764, 1985.

Cushman-Roisin, B., E. P. Chassignet, and B. Tang, Westward motion of mesoscale eddies, *J. Phys. Oceanogr., 20*, 758-768, 1990.

Elliott, B. A., Anticyclonic rings in the Gulf of México, *J. Phys. Oceanogr., 12*, 1292-1309, 1982.

Evans, R., K. Baker, O. Brown, and R. Smith, Chronology of warm-core ring 82B, *J. Geophys. Res., 90*, 8803-8811, 1985.

Ichiye, T., Circulation and water mass distribution in the Gulf of México, *Geofís. Int., 2*, 47-64, 1962.

Killworth, P. D., On the motion of isolated lenses on a betaplane, *J. Phys. Oceanogr., 13*, 368-376, 1983.

Kirwan, A. D., J. K. Lewis, A. W. Indest, P. Reinersman, and I. Quintero, Observed and simulated kinematic properties of loop current rings *J. Geophys. Res., 93*, 1189-1198, 1988.

Nof, D., On the interaction between thin isolated eddies and longshore currents, *J. Phys. Oceanogr., 14*, 125-137, 1984.

Nof, D., Draining vortices, *Geophys. Astrophys. Fluid Dyn., 42*, 187-208, 1988a.

Nof, D., Eddy-wall interactions, *J. Mar. Res., 46*, 527-555, 1988b.

Pavía, E. G., and B. Cushman-Roisin, Modeling of oceanic fronts using a particle method, *J. Geophys. Res., 93*, 3554-3562, 1988.

Pavía, E. G., and B. Cushman-Roisin, Merging of frontal eddies, *J. Phys. Oceanogr., 20*, 1886-1906, 1990.

Pavía, E. G., and M. López, Long-term evolution of elongated warm eddies, *J. Phys. Oceanogr., 24*, 2201-2208, 1994.

Pierrehumbert, R., A family of steady, translating vortex pairs with distributed vorticity, *J. Fluid Mech., 99*, 129-144, 1980.

Rossby, C. G., On displacements and intensity changes of atmospheric vortices *J. Mar. Res., 7*, 175-187, 1948.

Shi, Ch., and D. Nof, The destruction of lenses and generation of wodons, *J. Phys. Oceanogr., 24*, 1120-1136, 1994.

Vukovich, F. M., B. W. Crissman, M. Bushnell, and W. J. King, Some aspects of the oceanography of the Gulf of Mexico using satellite and in situ data, *J. Geophys. Res., 84*, 7749-7768, 1979.

Vukovich, F. M., and E. Waddell, Interaction of a warm core ring with the western slope in the Gulf of Mexico, *J. Phys. Oceanogr., 21*, 1062-1074, 1991.

L. Zavala Sansón, Laboratory for Fluid Dynamics and Heat Transfer. Faculty of Physics. Eindhoven University of Technology. Postbus 513, 5600 MB, Eindhoven, Netherlands. (e-mail: luis@tng.phys.tue.nl)

F. Graef and E. Pavía, Centro de Investigación Científica y Educación Superior de Ensenada, A.P. 2732, Ensenada, Baja California, México. (e-mail: fgraef@cicese.mx; epavia@cicese.mx)

(Received November 26, 1997; revised June 12, 1998; accepted July 22, 1998.)